

# On the Formation of Cool, Non-Flowing Cores in Galaxy Clusters via Hierarchical Mergers

Jack O. Burns,<sup>1</sup> Patrick M. Motl,<sup>1</sup> Michael L. Norman<sup>2</sup> and Greg L. Bryan<sup>3</sup>

<sup>1</sup> *University of Colorado, Center for Astrophysics and Space Astronomy, Boulder, CO 80309*

<sup>2</sup> *University of California San Diego, Center for Astrophysics and Space Sciences, 9500 Gilman Drive, La Jolla, CA 92093*

<sup>3</sup> *University of Oxford, Astrophysics, Keble Road, Oxford OX1 3RH*

We present a new model for the creation of cool cores in rich galaxy clusters within a  $\Lambda$ CDM cosmological framework using the results from high spatial dynamic range, adaptive mesh hydro/N-body simulations. It is proposed that cores of cool gas first form in subclusters and these subclusters merge to create rich clusters with cool, central X-Ray excesses. The rich cool clusters do not possess “cooling flows” due to the presence of bulk velocities in the intracluster medium in excess of 1000 km/sec produced by on-going accretion of gas from supercluster filaments. This new model has several attractive features including the presence of substantial core substructure within the cool cores, and it predicts the appearance of cool bullets, cool fronts, and cool filaments all of which have been recently observed with X-Ray satellites. This hierarchical formation model is also consistent with the observation that cool cores in Abell clusters occur preferentially in dense supercluster environments. On the other hand, our simulations overproduce cool cores in virtually all of our numerical clusters, the central densities are high, and physical core temperatures are often below 1 keV (in contrast to recent observations). We will discuss additional preliminary simulations to “soften” the cool cores involving star formation and supernova feedback.

## 1. Adaptive Mesh Refinement (AMR) Simulations of Cluster Formation and Evolution

In this paper, we present numerical results from the simulation of the formation and evolution of clusters of galaxies in the larger, cosmological context. Our simulations are performed with a sophisticated code that couples an N-body algorithm for evolving the collisionless dark matter particles with an Eulerian hydrodynamics scheme that utilizes adaptive mesh refinement to attain high spatial resolution. We are interested in the interaction of realistic galaxy clusters with their environment and therefore simulate large volumes of space and must impose a cosmological model on our simulations. We have chosen a flat  $\Lambda$ CDM cosmology with the following parameters:  $\Omega_m = 0.3$ ,  $\Omega_b = 0.026$ ,  $H_0 = h 100 \text{ km s}^{-1} \text{ Mpc}^{-1} = 70$  and  $\sigma_8 = 0.928$ .

The simulations presented here derive from a sample of galaxy clusters from a computational volume 256 Mpc on a side. From a coarse resolution run of the full volume we identified regions where clusters form and rerun the simulation with the adaptive mesh framework deployed about each region of interest in turn. In Figure 1 we show the region of space around a cluster of interest that is evolved with dynamic spatial refinement. We use from 7 to 11 levels of refinement yielding a peak spatial resolution from 16 to 1 kpc. The dark matter particles have a mass resolution of  $10^9 h^{-1} M_\odot$ .

The Simulated Cluster Archive, an online archive of

simulated clusters of galaxies evolved in both the adiabatic limit and with radiative cooling, is available at <http://sca.nsa.uiuc.edu>. This archive provides interactive tools to examine, visualize and extract data from over 50 clusters.

## 2. Radiative Cooling Simulations

A majority of galaxy clusters have cooling times in their central, or core, regions that are short compared to the expected age of the cluster. To adequately simulate clusters, we must account for the loss of energy from the fluid to X-Ray radiation as it is precisely the core region that dominates the X-Ray properties of clusters. It is interesting, from a theoretical point of view, to compare a sample of numerical clusters evolved with radiative cooling only with the properties of observed clusters. Using a large sample helps to alleviate concerns about statistical noise in the simulated cluster properties. We would not expect these clusters to “look” like clusters observed with *Chandra* in detail. In particular there is no mechanism in the input model that could account for the lack of gas cooler than about 1-2 keV in cluster cores as recently reported by various authors (e.g. Sakelliou et al. 2002). Nevertheless, it is useful to examine in detail what the effect of radiative cooling is and how, specifically, the model fails in comparison to observed clusters. We may then take an incremental approach among the various plausible physical mechanisms at play in cluster cores, introducing each into the simulations in turn based on our *a priori* expectations for how

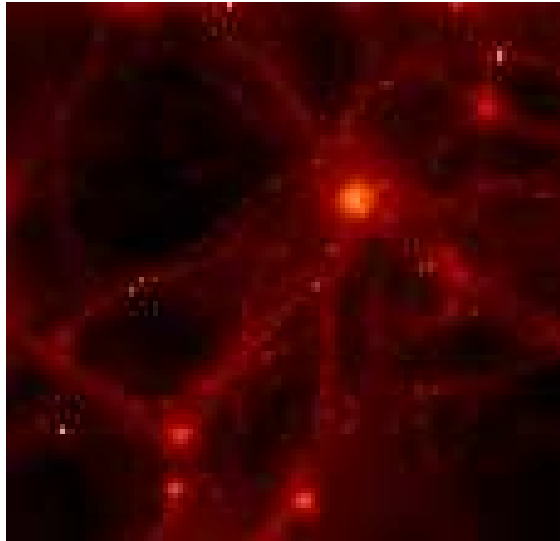


FIG. 1.— The region eligible for dynamic refinement for a typical cluster simulation. The region shown in the image is 36 Mpc on a side (out of the total computational volume with box length of 256 Mpc) while the inset highlighted region is 5 Mpc on a side.

the mechanism will correct the deficiencies of the previous iteration. For example, star formation, which will be considered later in this paper, acts as a highly selective sink of gas (Motl et al. 2003b). It removes only gas that is collapsing and rapidly cooling, the remainder of the fluid being largely unaffected. This property makes star formation an interesting process to consider in removing the gas cooler than 1 keV in cluster cores.

The loss of energy to radiation is calculated from a tabulated cooling curve derived from a Raymond-Smith plasma emission model assuming a constant metallicity of 0.3 relative to solar. The cooling curve is truncated below a temperature of  $10^4 K$ . Every timestep, we calculate the energy radiated from each cell and remove that amount of energy from the fluid (Motl et al. 2003a).

We have constructed a sample evolved with radiative cooling, comprising about 75 clusters in the mass range from  $4 \times 10^{14} M_{\odot}$  to  $2 \times 10^{15} M_{\odot}$ . To summarize this sample, we first examine the general appearance and typical histories of these simulated clusters. Recall from Figure 1 that we evolve the clusters along with their surrounding environment, including the network of filaments that intersect at nodes where clusters form. In Figure 2 we show a sequence of images demonstrating the interactions that are typically found in our sample clusters. This specific cluster is the most massive in our sample ( $M_{vir} = 2 \times 10^{15} M_{\odot}$  for an overdensity of  $\delta\rho/\rho = 200$ ). The cluster undergoes a major collision between approximately equal mass components that lasts for about 2 *Gyr* beginning at a redshift of  $z = 0.43$  with the initial collision of the cluster halos. The two cores make their closest approach at a redshift of 0.37 and begin to fall back toward one another at  $z = 0.31$ . Note in particular the strong shock fronts that expand out through the clusters and the tight cores of cooled gas behind the shocks. The cores survive this extreme collision intact and eventually merge into a single core at a redshift of approximately

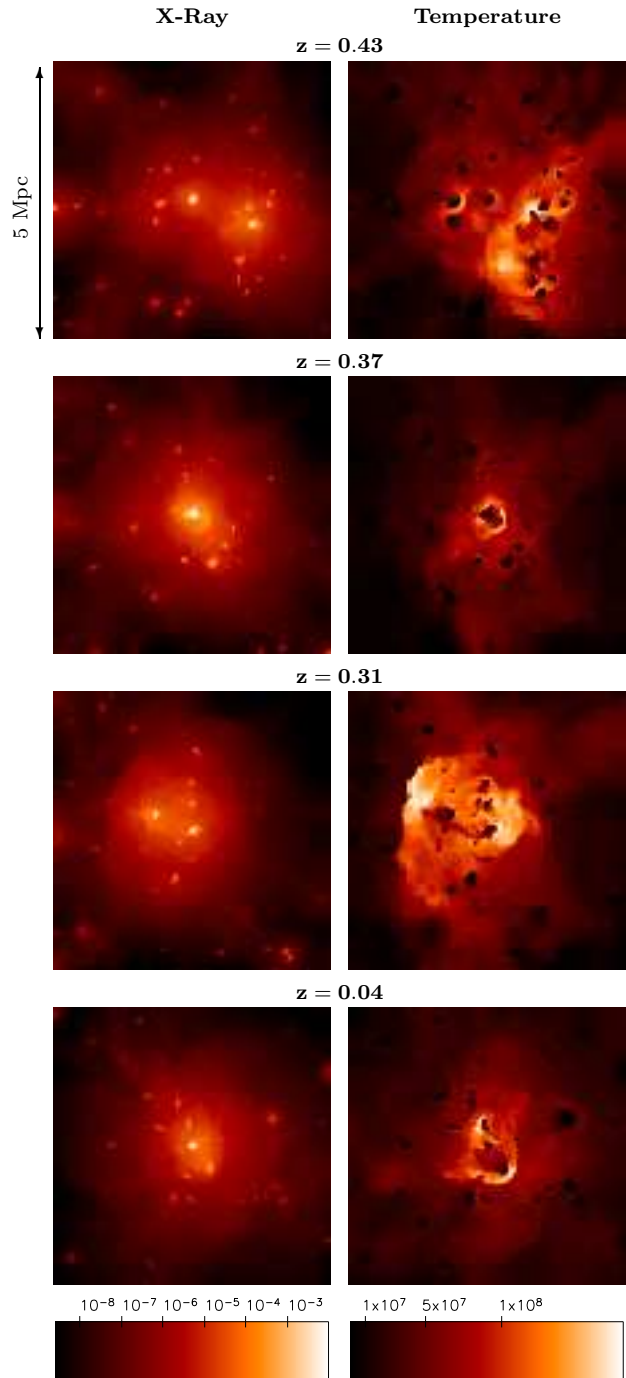


FIG. 2.— Three timeslices, depicting a major merger between two approximately equal mass clusters, are shown in the first three rows. The left column shows the predicted X-Ray surface brightness (normalized to its peak value) while the right column contains maps of the projected, emission-weighted temperature. The timeslices at redshifts of  $z = 0.43, 0.37, 0.31$  respectively correspond to the start of the merger, closest approach of the two cores and finally the cores reaching their turning point. A more typical interaction is shown in the bottom row, where a small subcluster (with mass of  $\approx 10\%$  the mass of the main cluster) falls through the cluster and its core is disrupted into an extended region of cooler gas behind the Mach cone of a shock front.

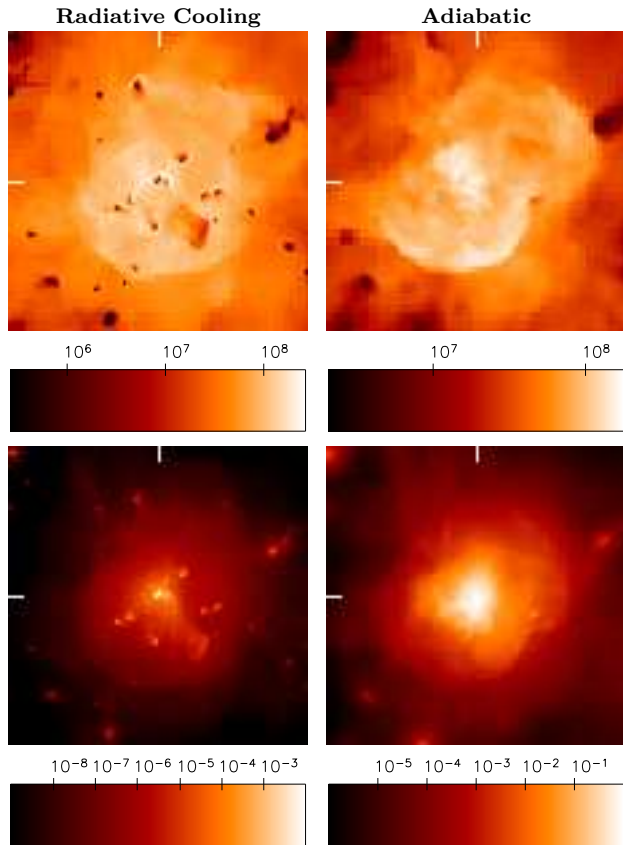


FIG. 3.— Comparison of radiative cooling (left column) and adiabatic (right column) realizations of the same cluster at the present epoch. The projected, emission-weighted temperature maps are shown in the top row while the bottom row contains synthetic images of the X-Ray surface brightness.

0.25. The full evolutionary sequence of this particular cluster is shown in an animation (Figure 5) that is available online at <http://casa.colorado.edu/~motl/research>.

In addition to major collisions, most clusters in our sample experience numerous interactions with subclusters that are less massive by a factor of 10 or more. An example of the impact of these more frequent interactions on the appearance of our simulated clusters is shown in the bottom panel of Figure 2. A small subcluster has fallen through the cluster from the upper left to bottom right in this projection. A strong shock front can be seen leading the subcluster’s core and this core material is being stripped to ultimately yield an extended patch of gas that is significantly cooler than the cluster average temperature. The subcluster decelerates so that the irregular patch is moving slowly compared to the cluster itself and the subcluster material quickly reaches pressure equilibrium with the cluster potential yielding a long lived, stable structure in the cluster’s temperature map.

In Figure 3 we show X-Ray surface brightness and temperature images from the same cluster evolved with radiative cooling and in the adiabatic limit to highlight the impact of radiative cooling. Both simulations begin

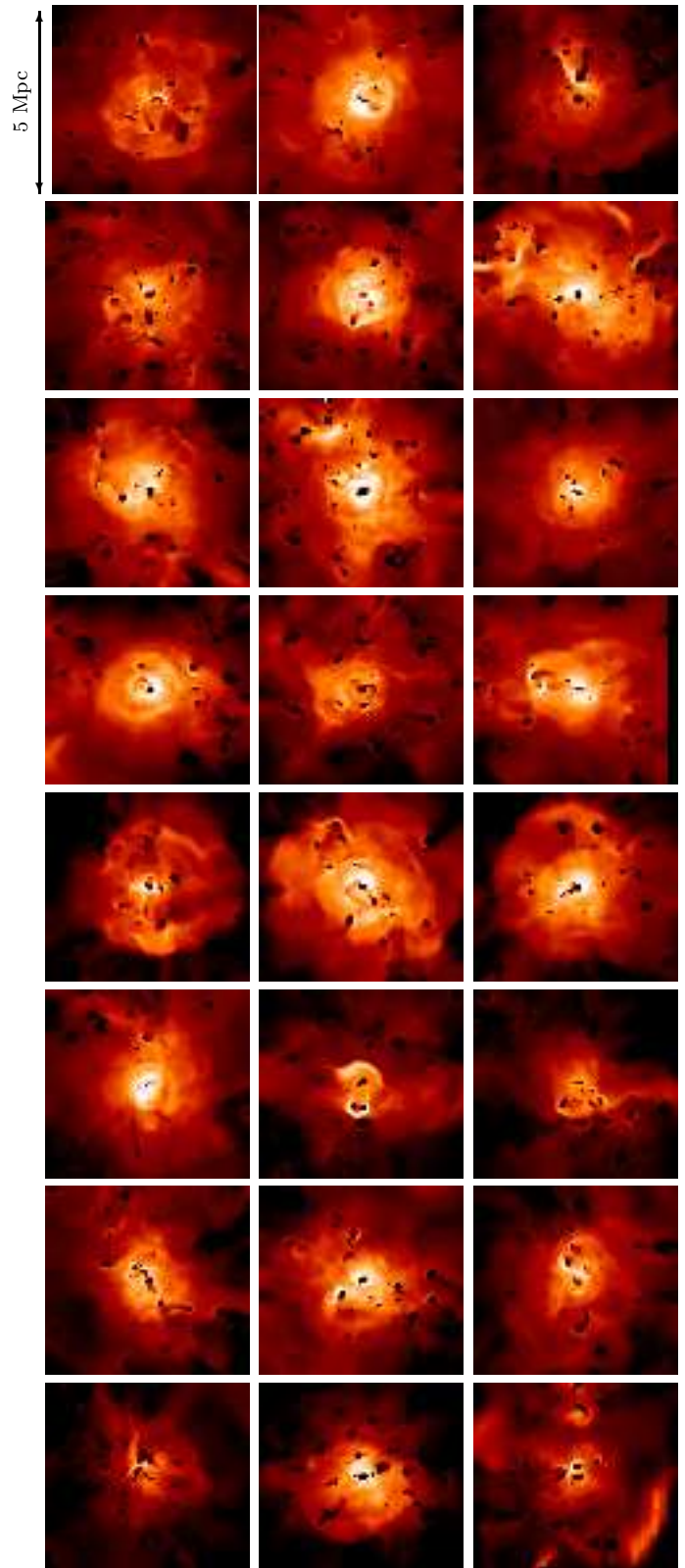


FIG. 4.— The projected, emission-weighted temperature maps for 24 clusters from the sample of radiative cooling clusters. Each image is 5 Mpc on a side and the clusters are arranged in order of decreasing mass through the table. The clusters show a wide variety of appearances ranging from strongly interacted to largely unperturbed and symmetric.

from identical initial conditions which means that the merger history is nearly identical for both clusters. The most dramatic difference between the two realizations is the presence of numerous cool cores when radiative cooling is introduced. These cores are dense (bright in the surface brightness map) and cool (dark in the temperature map) and significantly alter the cluster appearance on scales comparable to a typical core radius. In the adiabatic limit, these substructures quickly mix with the main cluster during interactions. With the addition of radiative cooling, the cool core in each substructure becomes a long lived entity that can survive a passage through the cluster. On larger scales, the temperature and density are in fact similar between the two simulations, for example, examine the curved shock front below the cluster center in both realizations. To lowest order, radiative cooling has an impact only in dense regions where the cooling time is short. To the next order, radiative cooling changes the interaction of subclusters within the cluster which results in strong, localized shocks and trails of stripped, cooler gas from the in-falling subcluster cores.

The range of structures in the radiative cooling clusters are shown in Figure 4 where we plot the projected, emission-weighted temperature maps at the present epoch from a subset of 24 clusters. The clusters are arranged in order of decreasing mass through the table with the most massive cluster ( $2 \times 10^{15} M_{\odot}$ ) in the upper left corner. Each image is centered on the cluster center of mass. The central cool cores vary widely in their strength (size) and shape (ranging from nearly spherical to bar-like to irregular filaments that connect multiple cores). Many of the clusters contain significant amounts of shocked gas from ongoing interactions and, in general, a large number of cool cores from previous interactions.

A typical cluster evolution from a redshift of 4 to the present day has been prepared as an animation. The still frames from the end of the animation are shown in Figure 5 where the projected, emission-weighted temperature and X-Ray surface brightness are shown for a region  $8 \text{ Mpc}$  on a side. The animation from this particular cluster evolution and other simulations are available online from <http://casa.colorado.edu/~motl/research>. This cluster gains most of its mass from one major collision (see also Figure 2 which shows additional images from this particular cluster) and undergoes numerous other interactions.

### 2.1. What Cooling Does

With radiative cooling, we have seen that subcluster cores often merge with the existing core. This observation suggests a **new, hierarchical formation scenario for cool cores** where cores are built along with the cluster itself through the hierarchical structure formation process of the standard, cold dark matter model.

This hypothesis suggests that rich clusters with strong cool cores (those clusters with a large central surface brightness excess and strongly declining temperature profiles in their cores) should be found in dense super-

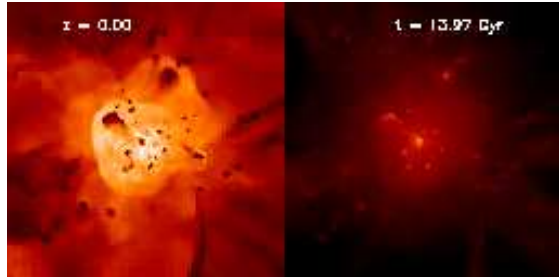


FIG. 5.— Still frames from the end of an animation showing the evolution of a massive cluster ( $2 \times 10^{15} M_{\odot}$ ) from redshifts of 4 to the present. The left panel shows the X-Ray surface brightness while the right panel shows the projected, emission-weighted temperature map for a region  $8 \text{ Mpc}$  on a side. The animation is available at <http://casa.colorado.edu/~motl/research> along with other movies from our simulations.

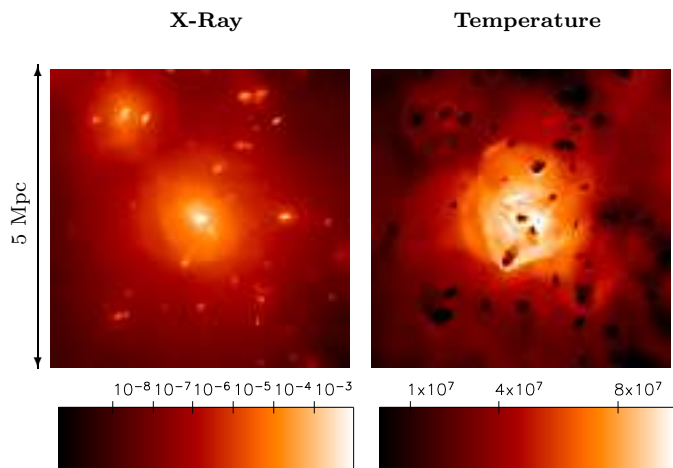


FIG. 6.— An example of the rich array of substructure present in the radiative cooling cluster sample at the present epoch. The X-Ray surface brightness and projected, emission-weighted temperature maps show numerous cool cores and the interaction of an in-falling subcluster with the main cluster.

cluster environments as these are the regions with the most cool fuel for the cluster core. Such a relationship has been found previously by Loken et al. (1999).

Significantly, the hierarchical formation scenario for cool cores naturally accounts for the rich substructure seen with high-resolution X-Ray instruments such as *Chandra* and *XMM*. An example case of this rich substructure is shown in Figure 6. Predicted X-Ray surface brightness and projected, emission-weighted temperature maps at the present epoch are shown for this relatively high mass cluster ( $M_{\text{vir}} \approx 1 \times 10^{15} M_{\odot}$ ). The surface brightness is normalized to its peak value and please note the extreme contrast in the X-Ray image. If cast in terms of a typical observation, the rich substructure would largely be absent in the X-Ray. It is important to note that the complex and irregular temperature structure would be relatively easy to detect provided enough counts could be detected to extract and fit spectra for different spatial regions.

Many clusters have been found to possess extremely complex temperature distributions, even in cases when



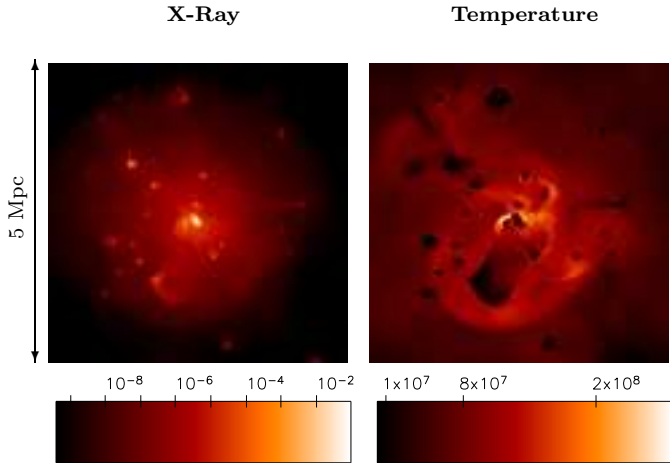


FIG. 7.— Demonstration of the formation of cold fronts in clusters of galaxies. A subcluster has fallen through the main cluster from the upper right and its gas has been stripped resulting in the sharp discontinuity separating cool and hotter gas to the lower left of the cluster center. The subcluster has decelerated and the leading shock front is no longer visible. Instead, there is now a relatively long-lived patch of cooler gas.

the X-Ray emission appears to arise from a symmetric, relaxed cluster. In some instances, the combination of the gas density and temperature indicates the presence of contact discontinuities in the central region of the cluster. Termed “Cold Fronts”, these features arise naturally from cluster mergers. An example from our simulations with radiative cooling only is shown in Figure 7. A small subcluster with mass  $\approx 0.1$  times the cluster mass has fallen through the cluster and the leading shock front has dissipated. Tidal forces and ram pressure stripping both act to disrupt the subcluster core and reshape the material into an extended patch of cooler gas. Since the virial temperature of subclusters will be significantly lower than that of the cluster, a similar process will act even in the adiabatic limit (Bialek et al. 2002) as the subcluster material is stripped from its dark matter halo and expands to reach pressure equilibrium with the cluster gas.

A table comparing snapshots from our simulations and recent X-Ray observations with *Chandra* is shown in Figure 8. There is a strong commonality between these observed features, including filaments, cold fronts and strong shocks from cluster-cluster collisions, and the structures seen in our simulations. As clusters form through hierarchical mergers, a process that continues to this day, the relatively X-Ray bright tracer material from cool cores is subjected to a complex flow through the cluster which results in a rich array of morphological features.

Radiative cooling enforces a scale length on halos, the relatively high density regions of cluster cores have short cooling times, and this breaks the self-similar scaling of cluster properties that would otherwise be present. In Figure 9 we show the  $L_X$  vs  $T$  relation for clusters from both our adiabatic and radiative cooling samples. The adiabatic clusters do indeed exhibit an  $L_X - T$  relation

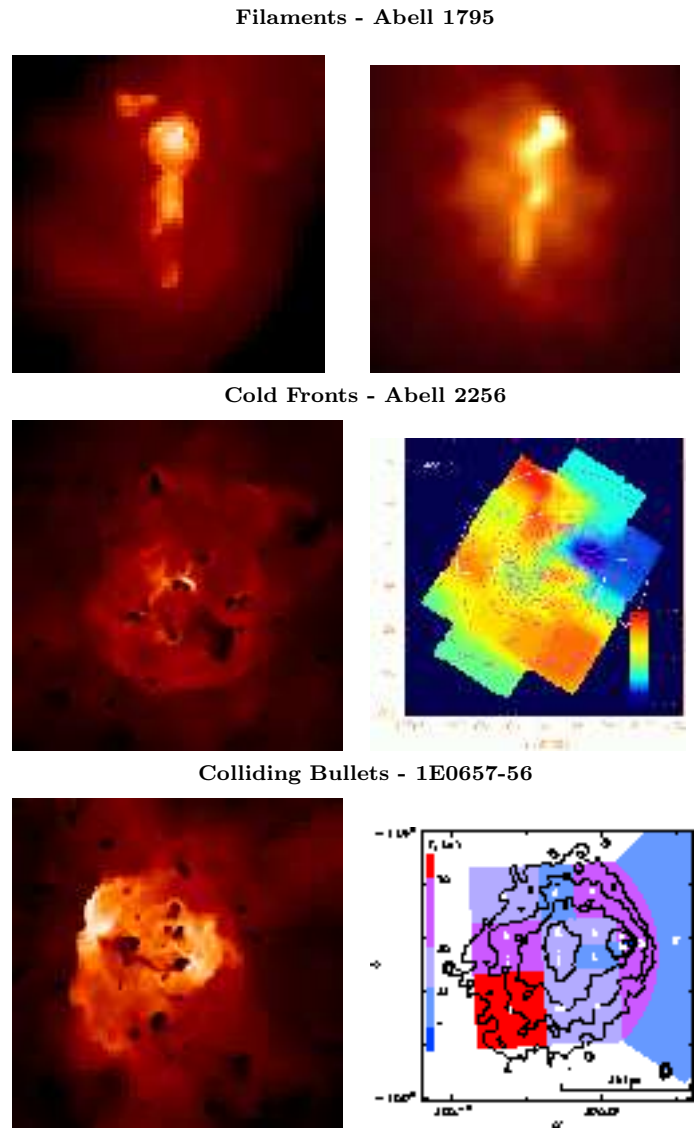


FIG. 8.— Comparison of features from cluster simulations (left) with recent observations from *Chandra* (right). In the right top row, we show the filament of cool gas trailing behind the core in Abell 1795 (Fabian et al. 2001). Complex, filamentary structures like this are common in our simulations and indicate the relative flow of material past the core. Many clusters, such as Abell 2256 (Sun, et al. 2002), show evidence for “Cold Fronts” when examined with high-resolution instruments such as *Chandra*. Similar, non-uniform temperature distributions are common features in our simulations. Finally, in the bottom row we show the high redshift cluster 1E0657-56 which, as reported by Markevitch et al. (2002), shows the collision between two clusters and a shock front centered on the small cool core that corresponds to a Mach number of approximately 2. For comparison, we show a major collision with similar Mach number between two approximately equal mass subclusters.

consistent with the self-similar scaling law. The radiative cooling clusters obey a steeper relation, closer to what has been observed, with the hottest and most massive clusters being over-luminous compared to the self-similar result and the cooler clusters and groups being under-luminous.

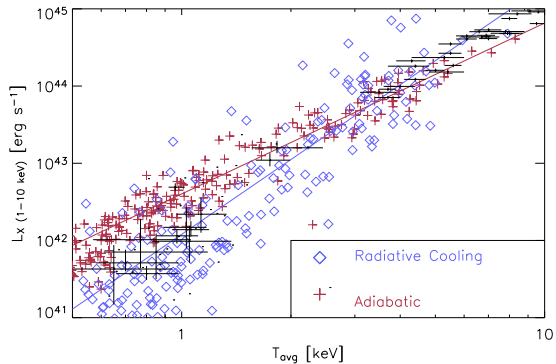


FIG. 9.— The relation between X-Ray luminosity and temperature for clusters from both the adiabatic and radiative cooling samples. The data points with error bars hotter than 2 keV are from Markevitch (1998) while the cooler cluster and groups are a random subset from the recent atlas of groups from Mulchaey et al. (2003). For the simulated clusters, the X-Ray luminosity is measured in the 1-10 keV energy band from all material within the virial radius of the cluster (taken to be the radius for an overdensity  $\delta\rho/\rho$  of 200) and the average cluster temperature is measured from the emission-weighted temperature within one half of a virial radius. The solid, colored lines show the least-squares fit relation for the 100 most massive objects in each sample. The adiabatic sample has a best fit slope of  $\approx 2$  while the radiative cooling sample has a steeper relation with a slope of  $\approx 3$ .

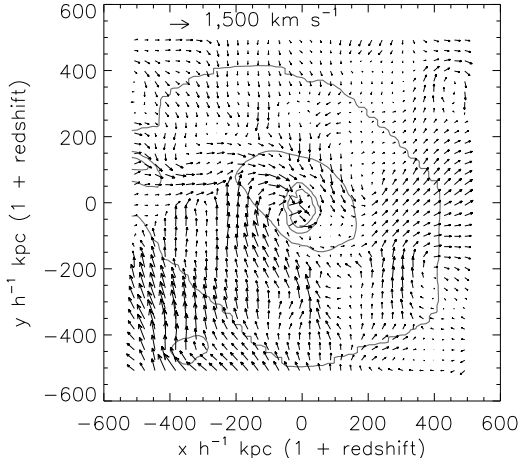


FIG. 10.— A two-dimensional slice of the velocity field from one particular cluster during a period free from major interactions. The contours are of the projected X-Ray emissivity. Note the large scale bulk flows through the cluster and the rotation of fluid in the core region.

An important question about our simulations is, “What is the fate of the cooling gas?”. If an idealized cluster were left in isolation and its atmosphere were allowed to cool it would inevitably form a “cooling flow” in its center. As the gas cools it loses pressure support and must flow inward in an attempt to regain hydrostatic equilibrium with the dark matter potential well.

The inflow pushes the gas to a higher density which only shortens the cooling time further. The solution is thus forced to be an inflow with more and more gas collapsing into the center of the cluster.

This scenario applies only to a cluster in isolation; recall from Figure 1 that we are considering clusters as they form in the larger cosmological environment. The filaments channel material into the cluster and impose complex flow boundary conditions that episodically bring discrete subclusters into the cluster in addition to the continuous inflow of warm, low density gas. The resulting flow field within clusters is very complex and the typical speeds are far in excess of the flow speeds expected to arise from the onset of a simple “cooling flow” model. An example velocity field from one of our clusters is shown in Figure 10 which depicts a slice through the velocity field in the central Mpc of the cluster. The last major collision for this cluster was approximately 2 Gyr in the past and from the contours in the X-Ray emission we see that cluster appears fairly relaxed. The isophotes are elliptical and there is twisting of the isophotes as one moves into the core region but there is no strong evidence for recent activity from the X-Ray data alone. When one examines the flow field, however, one sees that there are significant inflows from the lower and upper left corners of the frame, an outflow to the right and rotation as the in-falling material flows through the core. This flow corresponds to speeds often in excess of  $1,000 \text{ km s}^{-1}$ . Similar patterns are present in this particular cluster at other epochs and for other slices and for the remaining clusters in our sample as well.

## 2.2. Problems and What Radiative Cooling Alone Can Not Explain

We have seen that our simulations with radiative cooling have led to the hypothesis that cool cores in clusters of galaxies are formed through hierarchical mergers along with the cluster itself. As a consequence, we expect a variety of morphological features indicative of mergers to be present even in clusters with significant cool cores. These cool cores do not correspond to the picture of a cooling flow model, simply because of the cosmological infall of material into the cluster which enforces complex boundary conditions on the flow field. To summarize briefly, the cores contain cool gas but this gas is not at rest and is certainly not isolated from its environment.

The radiative cooling model can not be the last word in simulations of clusters, however. The model suffers from some serious deficiencies that must be addressed with more physically complete simulations. First, the radiative cooling only model over-produces cool cores and these cores are too robust and resilient during collisions and mergers. Nearly every dark matter potential well in our simulations is occupied by a halo of gas that has cooled significantly. As these halos merge and form clusters at the present epoch, the individual cores often survive and maintain an easily discernible identity independent of the cluster. While this is necessary to explain the irregular arrangement of gas in different temperature phases in clusters, the radiative cooling only model is too efficient in this respect as compared to observations.

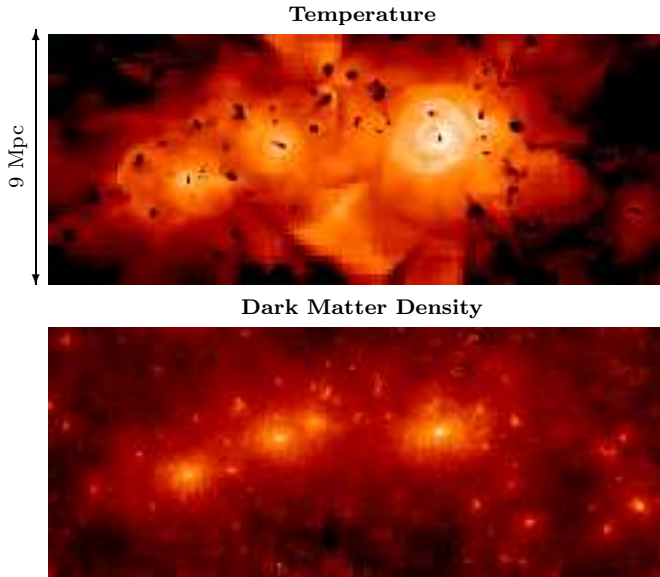


FIG. 11.— Projections of the emission-weighted temperature and dark matter particles from a rich supercluster region in our simulation volume. Essentially all potential wells formed by the dark matter particles are occupied by cores of cool gas in the radiative cooling simulations.

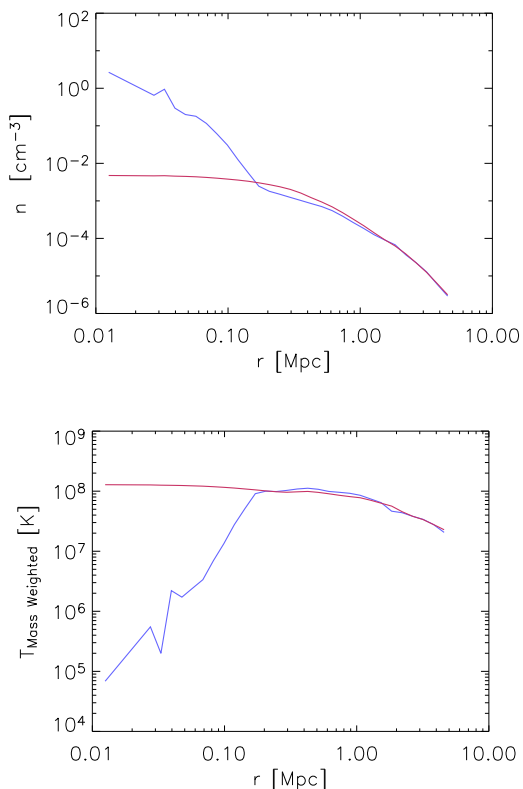


FIG. 12.— Spherically averaged profiles of the gas density and mass-weighted temperature from the same cluster evolved in the adiabatic limit (red curves) and with radiative cooling (blue curves). The cool core is evidenced as the cool, dense gas within the central 100 kpc.

For example, in Figure 11 we show the projected, emission-weighted temperature map and the corresponding projection of the dark matter particles for a large area containing a rich supercluster. There is an obvious correspondence between each dark matter halo and a steep decline in the gas temperature. The images also have many examples of interactions, none of which destroy the cool cores.

Why are the cool cores so resilient? With radiative cooling, the central density of the gas has been increased significantly as depicted in Figure 12. The cores are therefore akin to rigid billiard balls sloshing through the cluster medium. The steep density contrast shelters the cores from ram pressure stripping as subclusters rain in. As can also be seen in Figure 12, the temperature structure of the core gas contains material that is significantly cooler than  $1 \text{ keV}$ . This core material, if present in real clusters, would create spectral features in the UV and X-Ray that are not observed in any cluster.

A more complete computational model for galaxy clusters must address the following points. The cores must be softened in that they must be made less dense and therefore more susceptible to disruption during interactions. While a majority of clusters harbor cool cores there are definite examples of clusters that do not. With the correct input physics, a computational model for clusters will reproduce the observed abundance of cool cores at any epoch. A more daunting challenge is to account for the lack of gas at intermediate temperatures ( $1 \text{ keV} < T < 0.1 \text{ keV}$ ) in cluster cores.

### 3. Star Formation

Star formation should provide a natural mechanism to soften cool cores by both transforming dense, rapidly cooling gas into stars and also by heating the surrounding material with the energy injected from supernova explosions. We have incorporated the star formation prescription from Cen and Ostriker (1992) to introduce some of the effects of star formation in our simulations. The code examines all grid cells at the finest refinement level above a specified overdensity threshold. According to this star formation recipe, fluid is converted to collisionless “star” particles if the following conditions are met:

- The fluid is undergoing compression ( $\nabla \cdot \mathbf{v} < 0$ )
- Rapid cooling (local  $t_{cool} < t_{dyn}$ )
- The mass of fluid in the cell ( $m_b$ ) exceeds the Jean’s mass

When all conditions are met, a new star particle is created with a mass  $m_b \eta \Delta t / t_{dyn}$  and this amount of mass is removed from the fluid. The star formation rate is thus coupled to the local dynamical time,  $t_{dyn}$ , while  $\eta$  parameterizes the efficiency of star formation and  $\Delta t$  is the simulation timestep increment.

Once formed, the new star particle begins to deposit energy in the fluid to simulate the explosion of prompt, type II supernovae. The strength of supernova feedback is controlled by an efficiency,  $\epsilon_{feedback}$ , which gives the thermal energy injected by the star particle in terms of

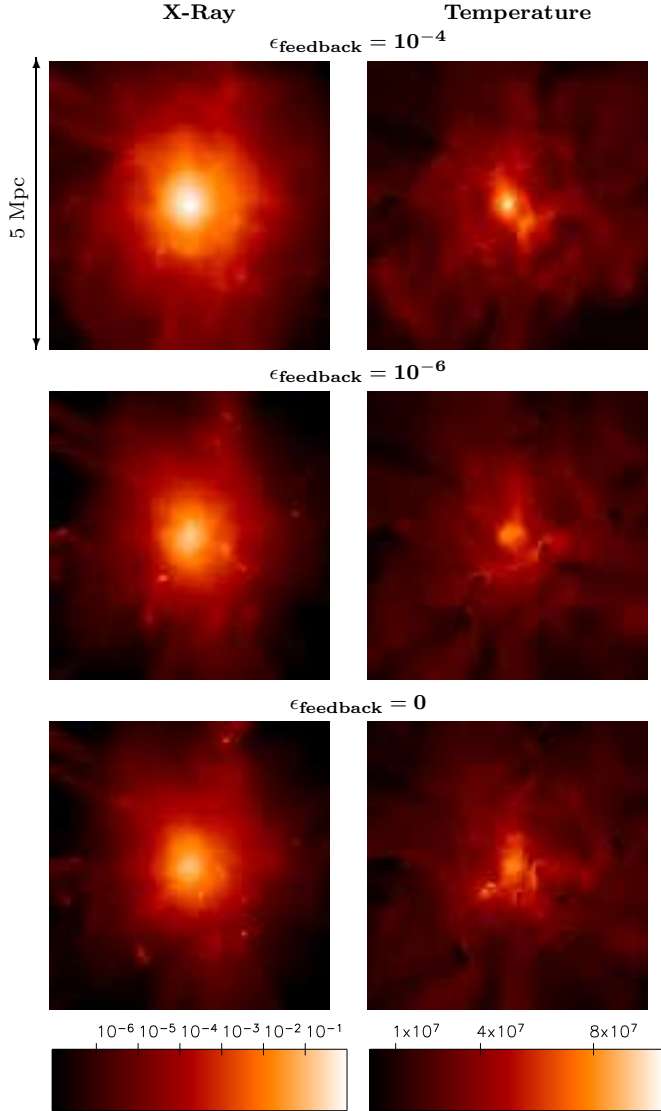


FIG. 13.— Comparison of a moderate mass cluster evolved with star formation and varying strength of thermal feedback,  $\epsilon_{feedback}$ , from an unrealistically large value in the top row, to a moderate value in the middle row, to the limiting case of no feedback in the bottom row. As the feedback strength is lowered, subclusters have stronger cool cores. The amount of gas converted to stars increases as the feedback strength is lowered, ranging from 2% to 20% to 33% for the case of zero feedback. The strength of feedback serves as a throttle on star formation and one generation of stars can disrupt (heat) gas in their local environment, preventing the formation of future generations.

the particle’s rest mass energy. The star particle also pollutes the fluid with a passive metallicity tracer field.

In our initial work with star formation, we explore the parameter space of the star formation model and assume that star formation continues to the present epoch.

The dominant parameter in the star formation model is the strength of supernova feedback. This parameter controls the condition of the fluid in star forming regions and largely dictates the amount of baryons converted into stars. In Figure 13 we show the end states for a test clus-

ter evolved with three different values for the strength of supernova feedback (from top to bottom in Figure 13 the strength varies from  $\epsilon_{feedback} = 10^{-4}, 4 \times 10^{-6}, 0$ ).

The impact of the remaining model parameters is less important. The overdensity threshold where star formation begins in the simulation and the efficiency of star formation,  $\eta$ , will impact the amount of mass converted into stars, but to a lesser extent than the feedback strength.

It should be noted that none of the parameters significantly impact the clusters that ultimately form from the star-forming halos. The resulting clusters tend to be similar to their adiabatic realizations, there are no cool cores in any cluster, and the clusters obey self-similar scaling relations. To explain the absence of cool cores in simulations with continuous star formation, consider the limiting case where the strength of feedback has been set to zero. This is the case where all cooling baryons form stars and any material that would result in a cool core is simply removed from the gas phase. As the strength of feedback is increased, fewer and fewer baryons are transformed into stars. This is because gas is again removed from the cool phase but this time by heating from supernova in a previous generation of stars. The net effect is that, when star formation operates continuously throughout the simulation, any fluid element that could become a cool core is quickly removed from the fluid.

#### 4. Truncated Star Formation

The star formation model that we employ is simplistic in many respects, not the least of which is the fact that we must approximate a complex physical process operating on mass scales around a solar mass with a collective process operating on scales up to a billion times larger. The star formation prescription is also free-form in that you can not *a priori* impose the amount of fluid converted to stars or the magnitude of the star formation rate with time in the simulation.

However, it is well known that the star formation rate has declined in the interval from a redshift of one to the present and was likely approximately constant before that time (see for instance, Figure 14, where we reproduce the cosmological history of the star formation rate compiled by Steidel et al. (1999)). As a constraint on the simulations with star formation we may simply halt star formation at a given epoch,  $z_{truncation}$  and complete the simulation with radiative cooling only. This approach essentially approximates the curve in Figure 14 with a step function.

While this approach is rather crude, there clearly must be a value for  $z_{truncation} = z_{crit}$  where a given cluster has just enough cool gas to form a cool core at the present epoch. If star formation were allowed to continue on beyond  $z_{crit}$ , proto-clusters would be depleted of their cool gas and the resulting cluster would essentially be adiabatic. If star formation is halted before  $z_{crit}$ , cool cores would begin to be overabundant just as they are in the radiative cooling only simulations.

In Figures 15 and 16 we show results from a numerical experiment where we simulated an otherwise identical cluster with star formation truncated at a set of values



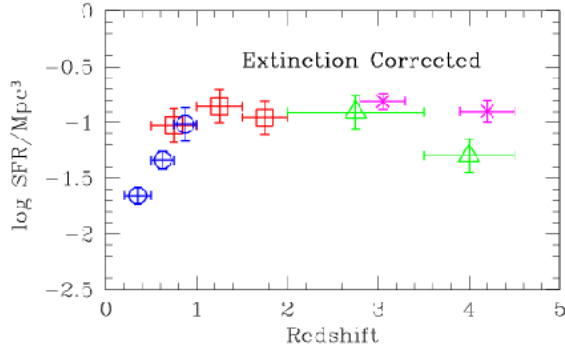


FIG. 14.— The inferred star formation rate from Steidel et al. (1999) after correction for extinction by dust. The star formation rate is consistent with a constant rate up to redshifts of approximately 1 and a subsequent decline in more recent time.

for  $z_{truncation}$ . In Figure 15 we can see the progression of the cluster’s appearance from the smooth, adiabatic realization to the highly structured cooling only realization as star formation is halted at higher and higher redshifts. From this experiment, this cluster has  $1.5 < z_{crit} < 2$ .

This result is emphasized in Figure 16 where the core temperature of the cluster is plotted against the value of  $z_{truncation}$ . The core temperature jumps abruptly from about 2 to 5 keV as the cool core disappears in this particular cluster.

It is encouraging that, for this limited experiment, the value of  $z_{crit}$  is reasonable in light of the results in Figure 14. First, the model is very simple and star formation does not decay, it is abruptly halted. Second, the results from Figure 14 at different epochs come from very different environments. At high redshifts, the star formation rate is indeed measured from the regions of high overdensity that likely will become clusters at the present day. For the lower redshift results, where the star formation rate is falling, these are measured in the dynamically younger field environment, not in clusters. It is therefore reasonable for the value of  $z_{crit}$  to exceed the value inferred for the field in the nearby universe.

## 5. Conclusions

To summarize our results for simulations with radiative cooling only, we find that the model of radiative cooling only can explain:

- The wide array of structures seen in recent X-Ray observations, including cool cores, filaments and rich substructure
- Formation and evolution of cool core clusters via accretion from supercluster filaments
- Agreement with observed cluster scaling relations such as the  $L_X$  vs  $T$  relationship
- Presence of cool cores but no inflows (no “cooling flows”) are present.

However, the radiative cooling only model can not be complete. Outstanding problems with the cooling only model include:

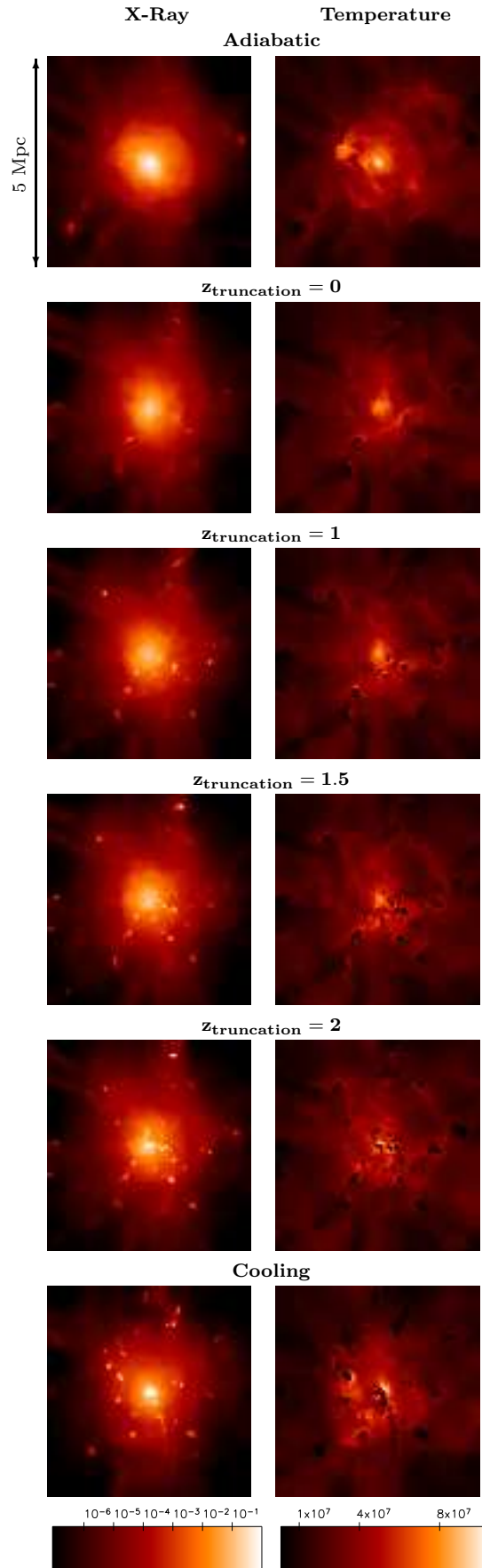


FIG. 15.— The X-Ray surface brightness and projected, emission-weighted temperature maps from the same cluster as in Figure 13 showing the Adiabatic, Radiative Cooling realizations as well as

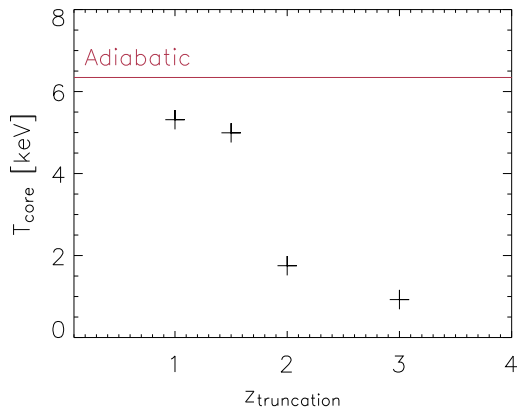


FIG. 16.— The core temperature from the same cluster evolved with star formation truncated at the indicated redshift. The core temperature is measured from the projected, emission-weighted temperature within a 50 kpc region centered on the system center of mass. For reference, the core temperature from the adiabatic simulation is also shown. This particular cluster undergoes an abrupt transition from having a cool core for values of  $z_{\text{truncation}} \geq 2$  and having no cool core for  $z_{\text{truncation}} \leq 1.5$  (see also Figure 15 for images of the clusters)

- Overabundance of cool cores (all clusters have cool cores).
- Core temperatures are  $< 1 \text{ keV}$ .

When star formation is introduced into our simulations, cool gas is rapidly channeled into stars leaving no gas to form the cool cores present in a majority of present day clusters. One promising approach in our simulations is to truncate star formation at a specific redshift as a means of approximating the observed decline in the universal star formation rate. We have found that star formation truncated at  $z < 2$  produces:

- Softer (low density) cool cores
- Core temperatures at observed levels ( $T_{\text{core}} \approx 1 - 2 \text{ keV}$ ).

This research was partially supported by grant TM3-4008A from NASA. The simulations presented were conducted on the Origin2000 system at the National Center for Supercomputing Applications at the University of Illinois, Urbana-Champaign through computer allocation grant AST010014N.

## References

- Bialek, J. J., Evrard, A. E., & Mohr, J. J. 2002, *ApJ*, 578, 9
- Fabian, A. C., Sanders, J. S., Ettori, S., Taylor, G. B., Allen, S. W., Crawford, C. S., Iwasawa, K., & Johnstone, R. M. 2001, *MNRAS*, 321, L33
- Loken, C., Melott, A., & Miller, C. J. 1999, *ApJ*, 520, 5
- Markevitch, M. 1998, *ApJ*, 504, 27
- Markevitch, M., Gonzalez, A. H., David, L., Vikhlinin, A., Murray, S., Forman, W., Jones, C., & Tucker, W. 2002, *ApJ*, 567, L27
- Motl, P. M., Burns, J. O., Loken, C., Bryan, G. L., & Norman, M. L. 2003, *ApJ*, *in press*
- Motl, P. M., Burns, J. O., Bryan, G. L., & Norman, M. L., 2003, *Proceedings of The Riddle of Cooling Flows in Galaxies and Clusters of Galaxies*
- Mulchaey, J. S., David, D. S., Mushotzky, R. F., & Burstein, D. 2003, *ApJS*, 146, 353
- Sakelliou, I., Peterson, J. R., Tamura, T., Paerels, F. B. S., Kaastra, J. S., Belsole, E., Böhringer, H., Branduardi-Raymont, G., Ferrigno, C., den Herder, J. W., Kennea, J., Mushotzky, R. F., Vestrand, W. T., & Worrall, D. M. 2002, *A&A*, 391, 903
- Steidel, C. C., Adelberger, K. L., Giavalisco, M., Dickinson, M., & Pettini, M. 1999, *ApJ*, 519, 1
- Sun, M., Markevitch, M., & Vikhlinin, A. 2002, *ApJ*, 565, 867